Eur. J. Mineral., 37, 819–828, 2025
https://doi.org/10.5194/ejm-37-819-2025

European Journal of Mineralogy
Open Access

The $M_2(PO_4)_2\Phi_8$ cyclic tetramer – a flexible structure-building unit – Part 1: Primary pegmatite phosphate minerals

Ian Edward Grey

CSIRO Mineral Resources, Private Bag 10, Clayton South, Victoria 3168, Australia

Correspondence: Ian Edward Grey (ian.grey@csiro.au)

Received: 3 June 2025 – Revised: 22 August 2025 – Accepted: 22 August 2025 – Published: 23 October 2025

Abstract. The minerals of the triphylite, alluaudite, zwieselite, and graftonite groups are amongst the most abundant of the primary phosphate minerals in granitic pegmatites. An analysis of the crystal structures of the four groups from the perspective of the connectivity between the metal atom polyhedra and the PO_4 tetrahedra for the individual metal atom sublattices has resulted in the identification of structural motifs that are common to the four primary mineral groups. All four structure types contain 2-polyhedra-wide ribbons formed from corner linking of $M_2(PO_4)_2\Phi_8$ cyclic tetramers, oriented along [001]. The ribbons in the four structure types all have the same topology but correspond to different geometrical isomers due to different orientations of the tetrahedra and different pairs of polyhedral edges involved in the ribbon formation. In the alluaudite, zwieselite, and graftonite group minerals, the polymerised cyclic tetramer (PCT) ribbons are connected along [010] by octahedral edge sharing, giving the same topology of (100) layers, with correspondingly similar b and c unit-cell parameters for the structures of the three mineral groups. The same PCT ribbons are also present in arrojadite–dickinsonite group primary phosphates. The persistent presence of the same type of structural unit across several different mineral groups is related to the high flexility of the cyclic tetramers to adjust to different crystal chemistries by rotation and buckling about the polyhedral corner linkages.

1 Introduction

Using geometrical graph theory, Hawthorne (1983) enumerated the polyhedral clusters of composition $M_2(TO_4)_2\Phi_n$, for the restrictions of no polymerisation of tetrahedra, no edge or face sharing between octahedra and tetrahedra, and no unlinked polyhedra. In total, 14 graphical isomers were obtained, of which 11 had more than one geometrical isomer, giving a total of 38 clusters. Hawthorne was interested in applying the results to phosphate, arsenate, and sulfate minerals containing commonly encountered di- and trivalent cations. He was able to restrict the number of relevant clusters based on the conjecture that a more stable cluster will have the maximum number of anions having their bond-valence requirement satisfied. For $T = 5+$, $6+$ and $M = 2+$, $3+$, this reduced the number of clusters for consideration to four, which included one isomer of each of the compositions with $\Phi = 6$ to 9. Hawthorne noted that each of the four clusters formed the basis for an extended hierarchy of mineral structures, consistent with their high stability. In the case of the cluster $M_2(TO_4)_2\Phi_7$, shown in Fig. 1a, an unpolymerised form occurs in the mineral morinite, $Ca_2Na[Al_2(PO_4)_2F_4(OH)(H_2O)_2]$, and various polymerised forms occur in many minerals including copiapite, minyulite, olmsteadite, hureaulite, phosphoferrite, melonjosephite, and whitmoreite (Hawthorne, 1979).

Rupture of the corner linkage between the octahedra in $M_2(TO_4)_2\Phi_7$ gives another of the four stable clusters, $M_2(TO_4)_2\Phi_8$, shown in Fig. 1b. The cluster, with a cyclic 4-member ring, is very flexible due to the possibility of rotation about the corner linkages between the octahedra and tetrahedra. Rotation about the octahedral 4-fold axes in Fig. 1b changes the shape of the ring from rectangular to flattened rhomboid, while rotation about the longitudinal and transverse 2-fold axes gives tilting of the tetrahedra relative to the octahedra and buckling of the tetramer. This flexibility allows

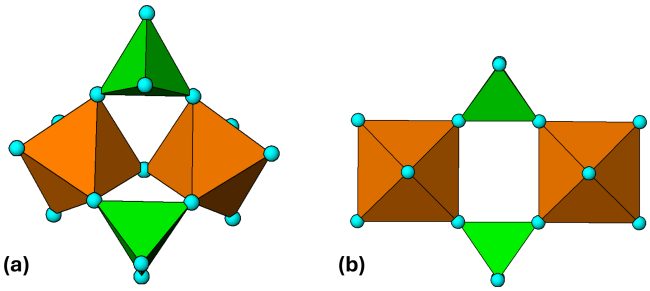

Figure 1. **(a)** $M_2(TO_4)_2\Phi_7$ cluster in morinite. **(b)** Ideal $M_2(TO_4)_2\Phi_8$ cluster with *mmm* point symmetry. All diagrams were prepared using ATOMS (Dowty, 2004).

the cluster to adjust readily to different H-bonding schemes and to interface with a wide range of other structural units. The $M_2(TO_4)_2\Phi_8$ cluster is best known in its linear chain form, where individual clusters join through pairs of corner-connected tetrahedra to give $M(TO_4)_2(H_2O)_2$, as in the mineral kröhnkite, $Na_2[Cu^{2+}(SO_4)_2(H_2O)_2]$ (Hawthorne and Ferguson, 1975). In a series of reviews and updates, Kolitsch, Fleck, and co-workers have classified dozens of natural and synthetic compounds containing kröhnkite chains, with compositions $A_nM(TO_4)_2 \cdot 2H_2O$, where $A = Ag^+$, Na^+, K^+, Rb^+, Cs^+, Tl^+, NH_4^+, H^+ or Ca^{2+} ($n = 1, 2$), $M = Mg^{2+}$, Mn^{2+}, Fe^{2+}, Co^{2+}, Ni^{2+}, Cu^{2+}, Zn^{2+}, Cd^{2+} or Al^{3+}, Fe^{3+}, Sc^{3+}, In^{3+}, Tl^{3+}, and $T = P^{5+}$, As^{5+} or S^{6+}, Se^{6+}, Cr^{6+}, Mo^{6+}, W^{6+} (Fleck et al., 2002; Fleck and Kolitsch, 2003, Kolitsch and Fleck, 2006). In addition to structures containing single chains, the authors have also described examples containing double chains and sheets. Minerals with composition $A_2M^{2+}(TO_4)_2 \cdot 2H_2O$, $T = P$, As and S have recently been formally approved as belonging to the kröhnkite supergroup, composed of the kröhnkite, talmessite, and fairfieldite groups (Hawthorne, 2025). The different groups have different dispositions of adjacent $M(TO_4)_2(H_2O)_2$ chains and different H bonding between the chains.

2 The $M_2(TO_4)_2\Phi_8$ cluster

Somewhat surprisingly, there does not appear to be a published example of an unpolymerised $M_2(TO_4)_2\Phi_8$ cluster with $T = P$ or As. For $T = S$, however, there are several minerals, with compositions $M^{2+}SO_4 \cdot 4H_2O$, M = Co, Zn, Cd, Mg, Mn, Fe, that have structures containing isolated cyclic tetramers, interconnected only by H bonding. The minerals form the rozenite ($M = Fe^{2+}$) group, the structure of which was determined by Baur (1962). The monoclinic structure ($P2_1/n$; $a = 5.979$, $b = 13.648$, $c = 7.977$ Å, $\beta = 90.43°$) is illustrated in projection along [100] in Fig. 2.

While the topology of the cluster in rozenite is the same as that for the ideal cluster with *mmm* point symmetry shown in Fig. 1b, the geometry is quite different due to rotations and tilts of the polyhedra to optimise the cluster packing and

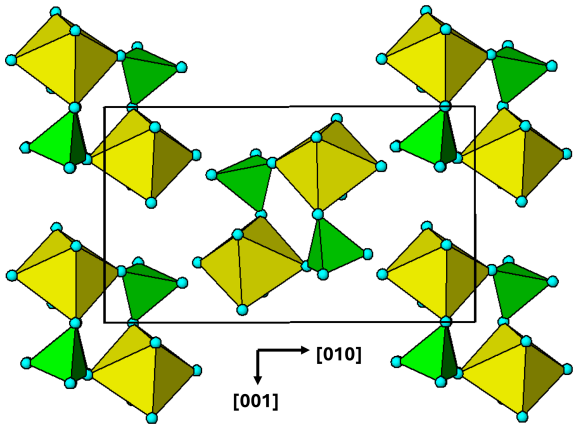

Figure 2. [100] projection of the rozenite crystal structure.

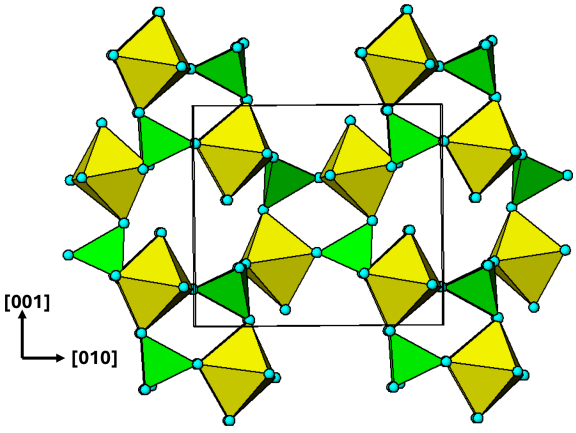

Figure 3. [100] projection of the crystal structure of phosphosiderite.

intercluster H bonding. The H-bonding scheme for rozenite has been reported by Meusburger et al. (2023).

Although the isolated cyclic tetramer is not known in phosphate minerals, the structure of phosphosiderite, $Fe^{3+}(PO_4) \cdot 2H_2O$, is built from cyclic tetramers sharing corners with eight adjacent clusters (Moore, 1966), as shown in Fig. 3. The octahedra in each cluster share a corner with the tetrahedra of four surrounding clusters, and vice versa, resulting in the elimination of 4 H_2O per cluster.

If the cyclic tetramers corner-share both an octahedron and a tetrahedron with adjacent clusters, a 2-octahedra-wide ribbon is obtained. This ribbon corresponds to a segment of the pinwheel structures of 120° intersecting kröhnkite chains as described by Moore (1973a), illustrated in Fig. 4 for the phosphate mineral example of brianite, $Na_2CaMg(PO_4)_2$, isostructural with merwinite (Moore and Araki, 1972). This ribbon, or derivatives of it, are found in several primary pegmatite phosphates, including triphylite–lithiophilite, alluaudite group minerals, zwieselite–triphylite, and graftonite–beusite.

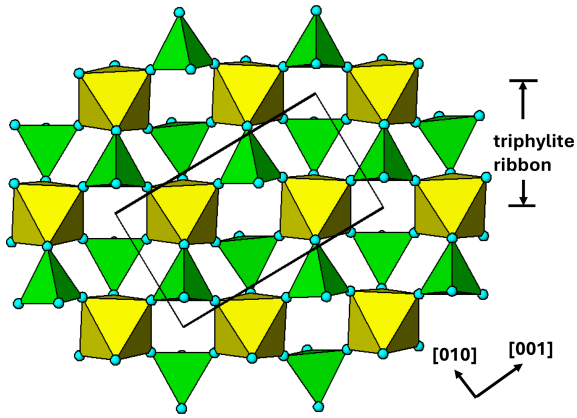

Figure 4. (100) section through the crystal structure of brianite.

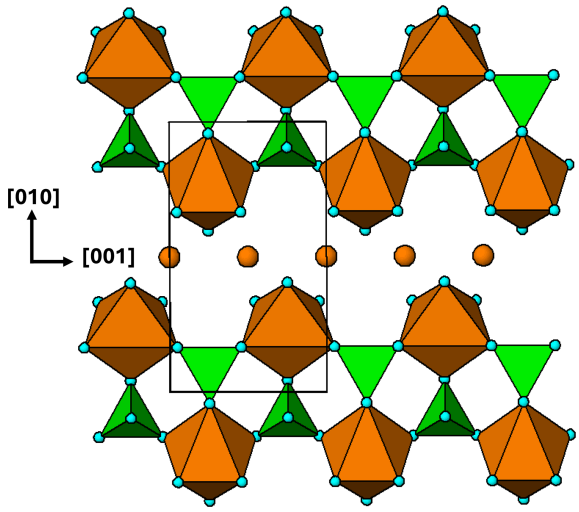

Figure 5. (100) layer of the triphylite–heterosite-sarcopside structure. The brown circles correspond to octahedral sites occupied by Li in triphylite, vacancies in heterosite and alternating Fe^{2+} and vacancies in sarcopside.

In the following sections we review the occurrence of the polymerised cyclic tetramer (PCT) in the above primary phosphate minerals. Of these, triphylite–lithiophilite provides the widest range of hydrothermal and low-temperature secondary phosphate products. In a companion paper (Part 2) we will report on the continuity of PCTs through the alteration sequences of the triphylite–lithiophilite primary phosphates.

3 Extended cyclic tetramers in primary pegmatite phosphate minerals

3.1 Triphylite and other olivine-derivative structures

Moore (1982) has noted that by far the greatest number of metasomatic and secondary pegmatite phosphates derive from the triphylite, $LiFe^{2+}(PO_4)$–lithiophilite, $LiMn^{2+}(PO_4)$ series of primary minerals. Members of the solid-solution series have olivine-derived orthorhombic crystal structures, *Pbnm*, with $a \sim 4.7$, $b \sim 10.3$, $c \sim 6.0$ Å (Losey et al., 2004). High-temperature hydrothermal leaching of lithium, with oxidation of the divalent cations, converts triphylite to heterosite, $Fe^{3+}PO_4$, and lithiophilite to purpurite, $Mn^{3+}PO_4$, which retain the same structure and space group. Lower-temperature alteration products are generally formed from intermediate compositions (ferrisicklerite) that have a mixture of di- and trivalent cations and retain some lithium. The primary mineral sarcopside, $Fe_3^{2+}(PO_4)_2$, has a small monoclinic distortion of the triphylite structure (Moore, 1972). It is related to triphylite by the cation exchange reaction $Fe^{2+} + \square \leftrightarrow 2Li^+$ and results in an alternation of Fe and vacancies at the octahedral sites occupied by Li in triphylite. Sarcopside is often found as an exsolution phase in lamella intergrowth with triphylite (Hatert et al., 2007).

A polyhedral representation of a (100) layer of the triphylite/heterosite/sarcopside structure is shown in Fig. 5. Cyclic tetramers are linked into ribbons along [001]. Each Fe-centred octahedron forms tetramers on *cis* pairs of edges, in contrast to kröhnkite chains, where the tetramers link through *trans* edges to form linear chains. In each tetramer, the tetrahedra are rotated by 90° about their tetramer edge relative to the ideal tetramer shown in Fig. 1b. This is a constraint imposed by the M and T atoms in triphylite occupying sites in a hexagonal close-packed anion lattice.

3.2 The alluaudite supergroup minerals

The alluaudite supergroup minerals have the simplified structural formula $A(2)'A(1)M(1)M(2)_2(TO_4)_3$, where $A(2)' =$ Na, K, $\square$; $A(1) =$ Na, Mn, Ca; $M(1) = Mn^{2+}$, Fe^{2+}; $M(2) = Fe^{2+}$, Fe^{3+}, Mn, Mg, Li; and $T =$ P, As, and monoclinic symmetry, C2/c or $P2_1/n$, with $a \sim 12$, $b \sim 12.5$, and $c \sim 6.5$ Å, $\beta \sim 115°$ (Hatert, 2019). Opinion is divided over whether alluaudites are primary minerals or are formed as Na–Li metasomatic alteration products of triphylite–heterosite. Moore (1971) reported alluaudites as fine-grained replacement products from triphylite, lithiophilite, and heterosite at numerous different pegmatite locations, and his observations were supported by other studies, e.g. Huvelin et al. (1972), Roda et al. (1996), and Fransolet et al. (1985). On the other hand, studies by Fransolet et al. (1998, 2004) support the formation of alluaudites as primary minerals, and Hatert et al. (2014) have prepared single-phase alluaudites by hydrothermal synthesis and established their stability field. Alluaudite supergroup minerals undergo high-temperature coupled oxidation/alkali leaching reactions analogous to those in triphylite–heterosite, with $Fe^{3+} + \square \leftrightarrow Fe^{2+} +$ Na, and the iron oxidation occurs at the $M2$ site. This has been taken into account in a new nomenclature scheme for the alluaudite supergroup where, for example, the end-member formula for alluaudite is $\square NaMnFe_2^{3+}(PO_4)_3$, and

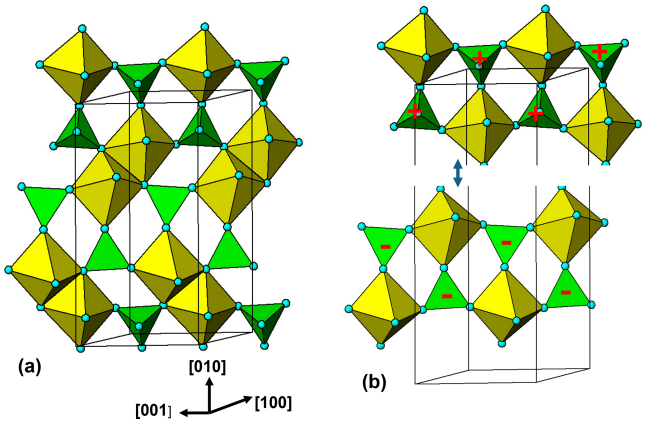

Figure 6. **(a)** (100) layer of $M(2)$-centred octahedra and PO_4 tetrahedra in alluaudite structure. **(b)** Cleaving of octahedral edge sharing to illustrate that the layer is composed of 2-octahedra-wide polymerised cyclic tetramers. Orientations of tetrahedra shown by + and −.

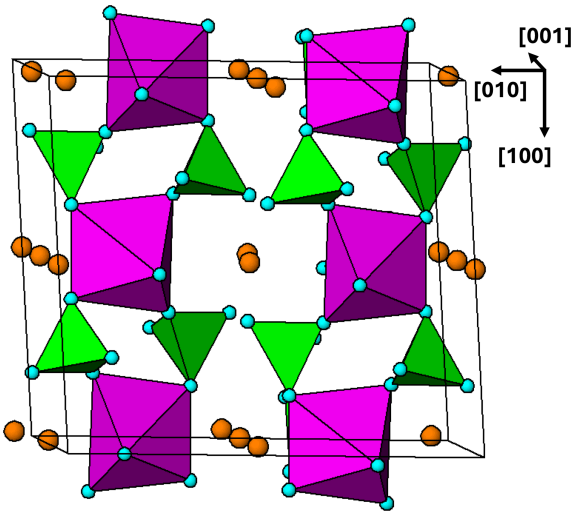

Figure 7. Projection along approximately [001] of the $M(1)$ octahedral substructure in alluaudite, showing (10-1) planes of corner-connected $M(1)$-centred octahedra and PO_4 tetrahedra. Brown circles are Na atoms.

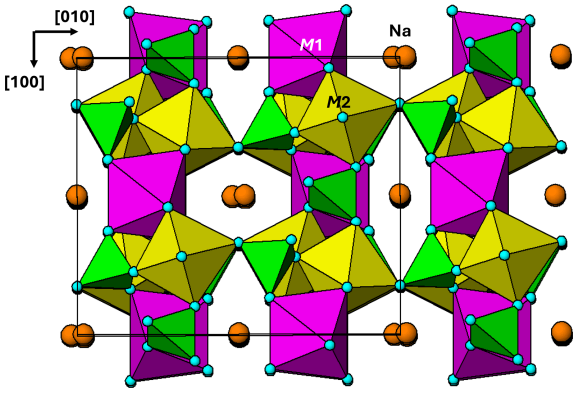

Figure 8. [001] projection of the alluaudite-type structure.

hagendorfite has a valency-imposed double-site occupancy at $M2$, giving $Na_2Mn(Fe^{2+}Fe^{3+})(PO_4)_3$ (Hatert, 2019).

The crystal structure of alluaudites is usually described in terms of [10-1] kinked chains of edge-shared $M(1)$- and $M(2)$-centred octahedra that are interconnected into (010) layers via corner sharing with PO_4 tetrahedra. The stacking of the layers along [010] results in large channels along [001] that are occupied by the $A(1)$ and $A(2)'$ cations. Moore (1971) noted that "the alluaudite structure type is not even remotely related to that of triphylite". If, however, the substructures associated with the sites $M(1)$ and $M(2)$ are separately considered, then a relationship to the triphylite structure emerges.

Figure 6a shows the $M(2)$-octahedral substructure. Pairs of octahedra share an edge and the dimers corner-link with PO_4 tetrahedra to form layers parallel to (100). The arrangement can be described as being built from 2-octahedra-wide polyhedral ribbons along [001] that are fused into (100) layers by octahedral edge sharing. The ribbons are shown in Fig. 6b. They have the same topology as the [001] ribbons in triphylite/heterosite shown in Fig. 5. The alluaudite ribbon is a geometrical isomer of the triphylite ribbon where the *cis* pairs of octahedral edges involved in the tetrameric rings lie in an equatorial plane of the octahedron for alluaudite but in an octahedral face for triphylite. To go from one to the other involves bond breaking and a rotation of the octahedra by $\sim 45°$. This results in an expansion of the chain periodicity from $c \sim 6.0$ Å in triphylite type to $c \sim 6.5$ Å in alluaudite type.

The $M(1)$ octahedral substructure is shown in projection approximately along [001] in Fig. 7. It comprises kröhnkite-type linear chains along [101], with no connection between adjacent chains. The (10-1) planes of kröhnkite-type chains are almost orthogonal (82°) to the (100) planes containing the $M(2)$ octahedral dimers as shown in the [001] projection of the complete structure in Fig. 8. At the intersections of the chains with the (100) layers, the $M(1)$-centred and $M(2)$-centred octahedra both share corners with common PO_4 tetrahedra to form intersecting cyclic tetramers.

3.3 Zwieselite–triplite minerals

Solid-solution members between zwieselite, $Fe_2^{2+}(PO_4)_2F$, and triplite, $Mn_2^{2+}(PO_4)F$, occur as late-stage primary phases in numerous granitic pegmatites (Vignola et al., 2014), as well as metasomatic products (Heinrich, 1951; Moore, 1973b, Lottermoser and Lu, 1997)). The solid solutions also incorporate Mg and Ca substitution for the divalent cations and OH substitution for F. The minerals have monoclinic symmetry, $I2/a$, with $a \sim 12.0$, $b \sim 10.0$, $c \sim 6.5$ Å, and $\gamma \sim 107°$. The structure is built from mutually orthogo-

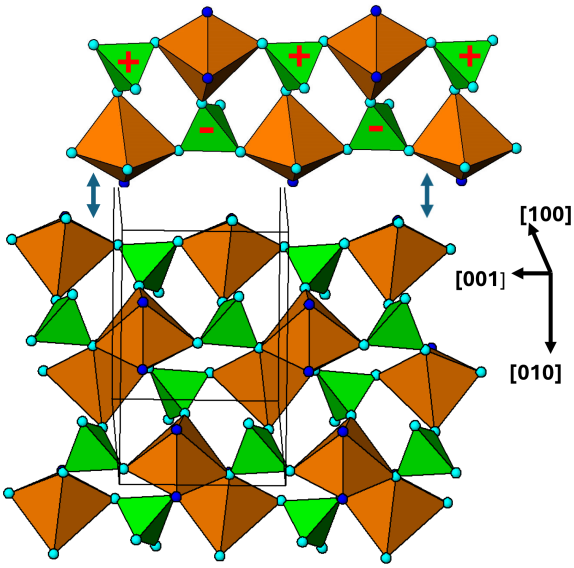

Figure 9. [100] projection of the $M2$ substructure in the zwieselite structure. A 2-octahedra-wide PCT ribbon is separated in the upper part of the diagram. Orientations of tetrahedra shown by the symbols + and −. The dark-blue circles correspond to F.

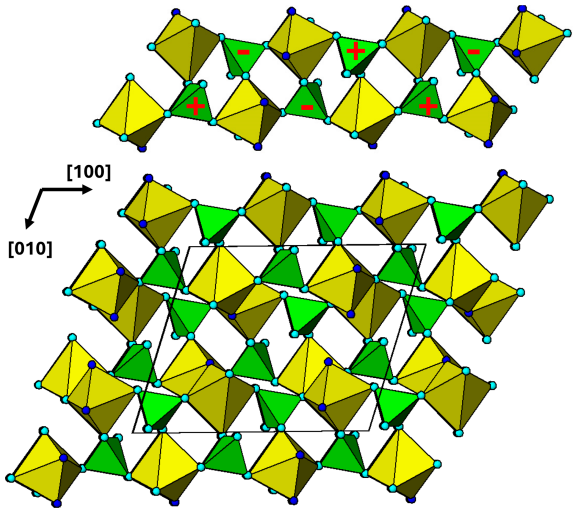

Figure 10. [001] projection of the $M1$ substructure in zwieselite. A 2-octahedra-wide PCT ribbon along[100] is separated in the upper part of the diagram. Orientations of tetrahedra shown by the symbols + and −. The dark-blue circles correspond to F.

nal [001] chains of edge-shared $M1$-centred octahedra and [100] zig-zag chains of edge-shared $M2$-centred octahedra. The octahedral chains are interconnected into 3D frameworks via corner sharing with PO_4 tetrahedra. Where the two types of interpenetrating octahedral chains intersect, pairs of $M1$-centred and $M2$-centred octahedra form approximately tetrahedral clusters by edge sharing. The clusters link into columns along [010] by further octahedral edge sharing, resulting in a dense structure. The density of zwieselite, $4.09\,g\,cm^{-3}$, is higher than the other primary phosphate minerals considered here, with densities in the range 3.63 to $3.79\,g\,cm^{-3}$ (Table 1).

As in the case of alluaudite, it is instructive to analyse the two metal atom substructures separately. The $M2$-centred octahedra and associated tetrahedra are viewed in projection along [100] in Fig. 9, and the corresponding $M1$-centred octahedra and connecting PO_4 tetrahedra are shown in projection along [001] in Fig. 10. The $M2$ substructure comprises 2-octahedra-wide PCT ribbons along [001], topologically the same as the [001] ribbons of $M(2)$-centred octahedra in alluaudite (Fig. 6). The chain periodicity along [001] of 6.5 Å is the same as that for alluaudite. The $M2$-based [001] ribbons in zwieselite are interconnected along [010] by edge sharing of the octahera, again, analogous to the $M(2)$ octahedral substructure in alluaudite. The shorter b axis of 10 Å in zwieselite relative to 12.5 Å in alluaudite is because the former has corner connection of *cis* anions on octahedral edges with PO_4 tetrahedra along [010], whereas the latter has corner connection of *trans*-axial anions of the octahedra with PO_4 tetrahedra.

The $M1$ substructure in zwieselite is also built from PCT ribbons, in this case oriented along [100] as shown in Fig. 10. Although topologically the same as the $M2$ substructure ribbons, the orientation of the tetrahedra results in a doubling of the chain periodicity to $2 \times 6.0 = 12.0$ Å. The shorter half-periodicity value of 6.0 Å, compared to the $M2$-based ribbon periodicity of 6.5 Å, is due to strong tilting of the polyhedra about [010] so that the alternating PO_4 and $M1O_4F_2$ polyhedra form crankshaft chains along [100] compared to linear chains for PO_4 and $M2O_4F_2$. In the $M1$ substructure, successive ribbons interconnect along [010] by edge sharing of the octahedra, as shown in Fig. 10. The $M1O_4F_2$ polyhedra shown in Fig. 10 are highly distorted with five bonds in the range 2.04 to 2.14 Å and the sixth distance, to a F, much longer at 2.63 Å. The $M2$ polyhedron is similar in having five bonds at 2.04 to 2.14 Å and a sixth bond, to F, at 2.44 Å (Yakubovich et al., 1978). Both polyhedra are more reasonably described as having $5 + 1$ coordination.

3.4 Graftonite–beusite primary minerals

Graftonite, ideally $Fe_3^{2+}(PO_4)_2$, and beusite, ideally $Mn_3^{2+}(PO_4)_2$, are end-members of a solid-solution series that also incorporates significant Mg and Ca. The members have monoclinic symmetry, $P2_1/c$, with $a \sim 8.8$, $b \sim 11.5$, $c \sim 6.15$ Å, $\beta \sim 99.2°$ (Tait et al., 2013). The structural formula is $M1M2M3(PO_4)_2$, where $M1$ is 7-coordinated, with $M1$–O bonds in the range 2.2 to 2.8 Å, and $M2$, $M3$ are 5-coordinated (Calvo, 1968; Tait et al., 2013). Ca and Mn are preferentially ordered at $M1$, up to essentially full occupancy by Ca (Wise et al., 1990). $M2 =$ Mn, Mg, Fe and $M3 =$ Mn, Fe (Tait et al., 2013). The crystal structure is gen-

Table 1. Crystal chemistry of iron-rich members of the triphylite, alluaudite, zwieselite, and graftonite group primary minerals.

	Triphylite (ref 1)*	Alluaudite (2)	Zwieselite (3)	Graftonite (4)
Formula	$Li(Fe_{0.89}Mn_{0.11})(PO_4)$	$(Na_{1.64}Ca_{0.13}Mn_{1.29}Fe^{2+}_{1.29}Fe^{3+}_{0.57}Mg_{0.04})(PO_4)_3$	$Fe_2(PO_4)F$	$(Fe_{1.65}Mn_{0.61}Ca_{0.58}Mg_{0.15})(PO_4)_2$
Space group	*Pbnm*	$C2/c$	$I112/a$	$P21/c$
a	4.6904	11.9721(9)	11.999(3)	8.7994(4)
b	10.2855(9)	12.5899(8)	9.890(3)	11.5702(5)
c	5.9871(4)	6.5029(5)	6.489(1)	6.1365(4)
β or γ		114.841(8)	107.72(2)	99.320(4)
Density ($g\,cm^{-3}$)	3.63	3.75	4.09	3.69
M–PO_4 polymerised cyclic tetramer (PCT) substructures	[001] 2-octahedra-wide PCT ribbons in (100) planes at $x = 0, 1/2$	$M1$ kröhnkite chains along [101]. $M2$ [001] PCT ribbons in (100) plane at $x = 1/4, 3/4$	$M1$ [100] PCT ribbons in (001) plane $M2$ [001] PCT ribbons in (100) plane at $x = 0, 1/2$	$M1$ [001] PCT ribbons in (100) plane at $x = 0$ $M2$ [001] PCT ribbons in (010) plane at $y = 0, 1/2$ $M3$ edge-shared cyclic tetramers forming (100) layers at $x = 1/2$
Linkage of PCT ribbons	Via edge sharing with Li-centred octahedra	Via edge sharing of $M2$ octahedra along [010]	Via edge sharing of $M1$ octahedra in [001] chains Edge sharing of $M2$ octahedra along [010]	Via edge sharing of $M1$ polyhedra along [010] Via pairs of PO_4 forming cyclic tetramers along [100]
Orientation of tetrahedra in PCT ribbons	$+-+-$	$M2$ $++++$ and $----$ in successive ribbons along [010]	$M1$ $++--++--$ $M2$ $+-+-$	$M1$ $++++$ and $----$ in successive ribbons along [010] $M2$ $+-+-$

* (1) Losey et al. (2004); (2) Redhammer et al. (2005); (3) Yakubovich et al. (1978); (4) Tait et al. (2013).

erally described as a dense 3D framework of polyhedra with extensive edge and corner sharing between PO_4 tetrahedra and the divalent metal-centred polyhedra. As for alluaudite and zwieselite, we consider the substructures associated with the different metal atoms.

The $M1$ substructure with associated PO_4 tetrahedra is in the form of (100) layers at $x = 0, 1$. A view normal to the layer is shown in Fig. 11. In this diagram the $M1$ polyhedron is shown as a distorted octahedron, by considering the six shortest $M1$–O bonds, in the range 2.2 to 2.5 Å. 2-octahedra-wide PCT ribbons are oriented along [001] and are interconnected along [010] by edge sharing of the $M1$-centred polyhedra.

The $M2$ substructure forms heteropolyhedral (010) planes at $y = 0$ and $1/2$. A representation of the layer at $y = 0$ is shown in Fig. 12. As for the $M1$ substructure, it comprises 2-octahedra-wide PCT ribbons along [001]. The ribbons are interconnected along [100] via pairs of PO_4 tetrahedra that link into cyclic tetramers by corner sharing with the octahedra in adjacent [001] ribbons. A comparison of the [001] ribbons in Fig. 9 ($M2$ in zwieselite) with those for graftonite in Fig. 12 shows that they have identical topologies as well as the same geometry of tetrahedral orientations.

The $M3$ substructure forms heteropolyhedral (100) layers, located halfway between the $M1$ substructure layers. The

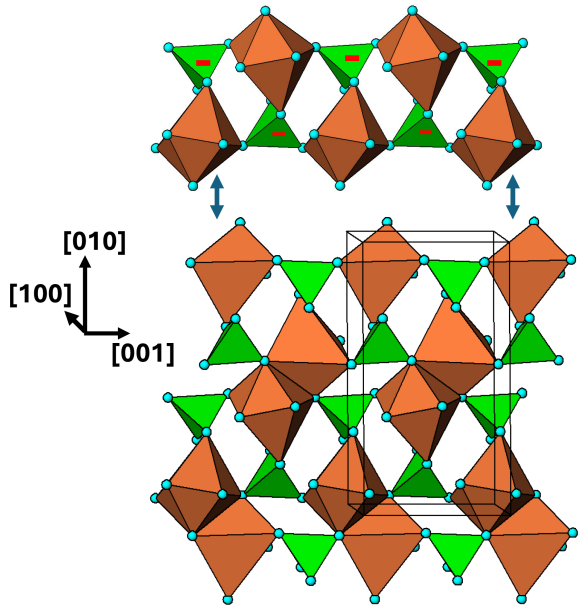

Figure 11. [100] view of the $M1$ substructure in graftonite. A 2-octahedra-wide PCT ribbon along [001] is separated above the structure. Orientations of tetrahedra shown by the symbols + and −.

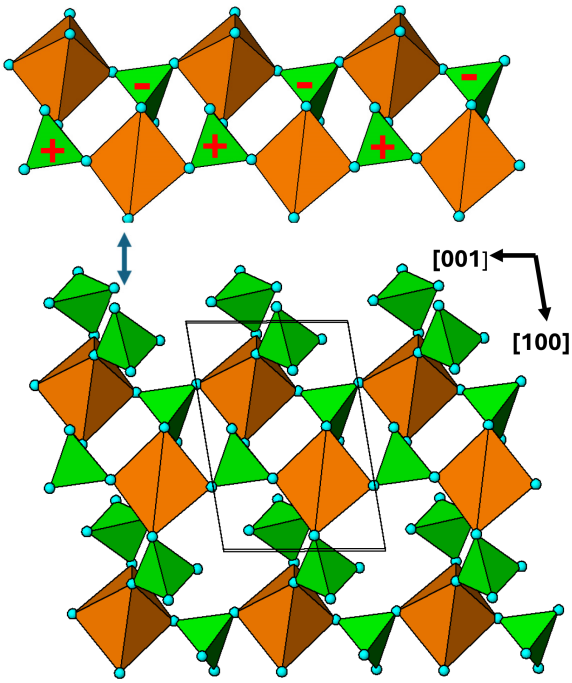

Figure 12. [010] view of the $M2$ substructure in graftonite. A 2-octahedra-wide PCT ribbon along [001] is separated above the structure. Orientations of tetrahedra shown by the symbols + and −.

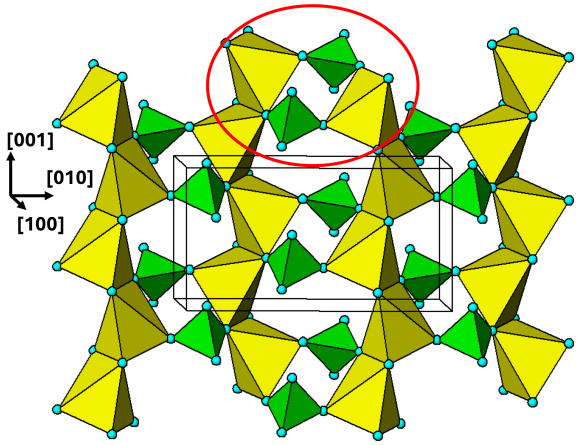

Figure 13. [100] view of the $M3$ substructure layer in graftonite at $x = 1/2$. One cyclic tetramer is outlined with the red ellipse.

$M3$ layer at $x = 1/2$ is shown in Fig. 13. The $M3$-centred polyhedra share edges to form chains along [001]. The chains are interconnected along [010] by pairs of PO_4 tetrahedra that form cyclic tetramers with the $M3O_5$ polyhedra. Each cyclic tetramer is connected to four other clusters by edge sharing of the polyhedra.

4 Discussion

The four mineral groups chosen for study, triphylite, alluaudite, zwieselite, and graftonite, are amongst the most abundant primary Fe–Mn phosphate minerals in granitic pegmatites. The crystal chemistry of each of the four groups has been discussed in detail by Losey et al. (2004) (triphylite–lithiophilite), Moore (1971), Hatert (2008, 2019), Tait et al. (2021) (alluaudites), Heinrich (1951), Roda-Robles et al. (2014), Vignola et al. (2014) (zwieselite–triplite), Tait et al. (2013), and Hawthorne and Pieczka (2018) (graftonite–beusite).

The focus in this study of considering the connectivity between the metal atom polyhedra and the PO_4 tetrahedra for the individual metal atom sublattices has resulted in the identification of structural motifs that are common to the four primary mineral groups studied. The crystal chemistry comparisons of the four mineral groups from this perspective are summarised in Table 1. All four structure types contain 2-polyhedra-wide ribbons formed from corner linking of $M_2(PO_4)_2\Phi_8$ cyclic tetramers. The PCT ribbons in the four structure types all have the same topology, whereby each polyhedron participates in two cyclic tetramers, involving *cis* pairs of octahedral edges in forming the rings. Each polyhedron shares corners with three PO_4 tetrahedra, and each tetrahedron in turn shares three corners with polyhedra in the ribbon, thus retaining the M / P atomic ratio of 1 as in the isolated cluster.

Several different geometrical isomers of the ribbon topology have been identified. These are mainly due to different orientations of the tetrahedra in the ribbons, labelled + and – in the figures, depending on the location of the apical anion of the tetrahedra, pointing up or down relative to the ribbon plane. The $M2$ ribbons in zwieselite and graftonite have the same tetrahedral orientation sequence $+-+-$ as in triphylite, whereas the $M2$ ribbons in alluaudite and the $M1$ ribbons in graftonite have all tetrahedra in the ribbons oriented the same way. The $M1$ ribbon in zwieselite has the sequence $++--++--$, with a corresponding doubling of the ribbon periodicity to 12 Å. Different geometrical isomers of the ribbon topology also result from different *cis* pairs of polyhedral edges involved in the ribbon formation, with the pairs of edges belonging to an octahedral face in triphylite and for $M1$ in graftonite (O–O–O angle $\sim 60°$) but to an equatorial plane of the octahedron in alluaudite and zwieselite and for $M2$ in graftonite (O–O–O angle $\sim 90°$).

The $M2$ PCT ribbons in alluaudite and in zwieselite and the $M1$ PCT ribbons in graftonite are all interconnected via edge sharing of the polyhedra along [010], giving the same topology of the (100) layers, which thus have related b and c cell parameters. The shorter c parameter for graftonite of 6.1 Å compared to 6.5 Å for the other two is due to the different *cis* pairs of polyhedral edges involved in the ribbon formation as described above. The relatively large difference in b for zwieselite, 9.9 Å compared with 11.6 and 12.6 Å for

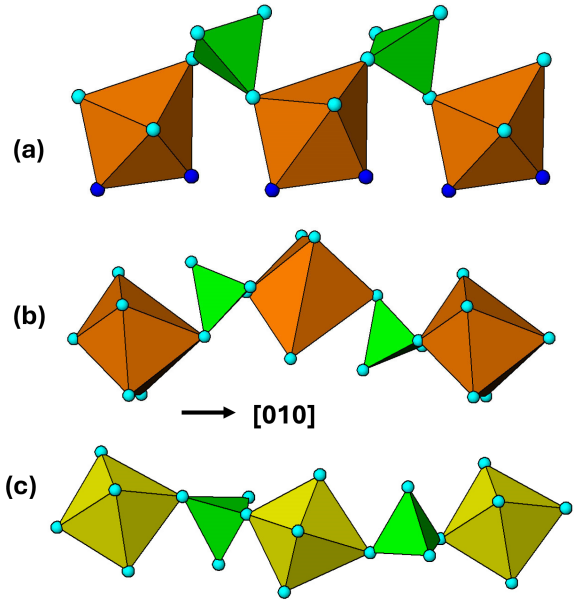

Figure 14. Heteropolyhedral corner linkages along [010] in **(a)** zwieselite, $M2$ polyhedra; **(b)** graftonite, $M1$ polyhedra; and **(c)** alluaudite, $M2$ polyhedra.

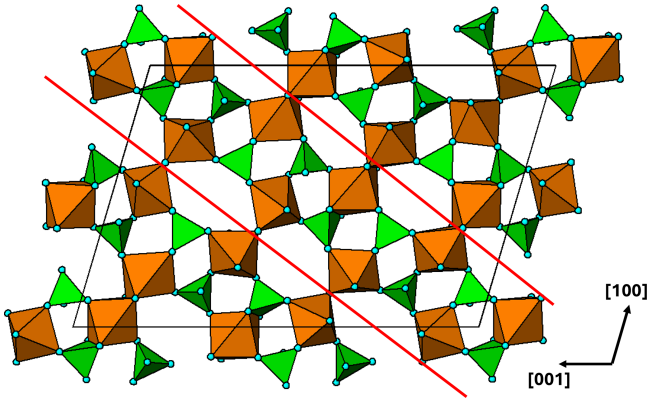

Figure 15. (010) heteropolyhedral layer at $y = 1/4$ in the arrojadite-type structure. The red lines delineate a [101] 2-octahedra-wide PCT ribbon.

the other two minerals, is due to the different modes of linkage of adjacent ribbons. The tetrahedra in adjacent ribbons connect via *trans* anions of the M polyhedra in alluaudite and graftonite but via *cis* anions (polyhedral edge) in zwieselite. This is illustrated in Fig. 14. The 1 Å difference in b between alluaudite and graftonite is due to different degrees of buckling of the heteropolyhedral linkages as shown in Fig. 14.

Although the study was restricted to the four primary mineral structure types, the same polymerised tetrameric clusters are also present in related primary phosphate minerals; for example the structures of the triploidite–wolfite series minerals (Waldrop, 1970) have the same clusters as the zwieselite–triplite series described here, and the wyllieite group of primary minerals (Moore and Molin-Case, 1974) has the same clusters as in alluaudites.

A preliminary examination has been made of the large, complex structure adopted by the arrojadite–dickinsonite group of primary minerals, $A_2B_2CaNa_{2+x}M_{13}Al(PO_4)_{11}(PO_3OH_{1-x})[F,(OH)]_2$ (Krutik et al., 1979; Tomes et al., 2018; de Wit and Mills, 2022). They have monoclinic symmetry, Cc, with $a \sim 16.5$, $b \sim 10.0$, $c \sim 24.5$ Å, and $\beta \sim 106°$. A plot of the (010) heteropolyhedral layer at $y = 1/4$ in Fig. 15 shows PCT ribbons along [101]. Adjacent ribbons are interconnected by both corner and edge sharing of the M-centred octahedra. Further studies of structures of the granitic pegmatite primary and high-temperature hydrothermally derived phosphate minerals using the focus of PCT cluster formation could be fruitful.

Code availability. All diagrams were prepared using ATOMS (Dowty, 2004).

Data availability. No data sets were used in this article.

Competing interests. The author has declared that there are no competing interests.

Disclaimer. Publisher's note: Copernicus Publications remains neutral with regard to jurisdictional claims made in the text, published maps, institutional affiliations, or any other geographical representation in this paper. While Copernicus Publications makes every effort to include appropriate place names, the final responsibility lies with the authors. Views expressed in the text are those of the authors and do not necessarily reflect the views of the publisher.

Review statement. This paper was edited by Cristian Biagioni and reviewed by Sergey Aksenov and Kimberly Tait.

References

Baur, W. H.: Zur Kristallchemie der Salzhydrate. Die Kristallstrukturen von $MgSO_4.4H_2O$ (Leonhardtit) und $FeSO_4.4H_2O$ (Rozenit), Acta Crystallogr., 15, 815–826, 1962.

Calvo, C.: The crystal structure of graftonite, Am. Mineral., 53, 742–750, 1968.

de Wit, F. and Mills, S. J.: Arrojadite-group nomenclature: sigismundite reinstated, Eur. J. Mineral., 34, 321–324, https://doi.org/10.5194/ejm-34-321-2022, 2022.

Dowty, E.: ATOMS for Windows, vsn. 6.1. Shape Software, Kingsport, USA, 2004.

Fleck, M. and Kolitsch, U.: Natural and synthetic compounds with krohnkite-type chains. An update, Z. Kristallogr., 218, 553–567, 2003.

Fleck, M., Kolitsch, U., and Hertweck, B.: Natural and synthetic compounds with krohnkite-type chains. Review and classification, Z. Kristallogr., 217, 435–443, 2002.

Fransolet, A.-M., Abraham, K., and Speetjens, J.-M.: Evolution genetique et signification des associations de phosphates de la pegmatite d'Angarf-Sud, plaine de Tazenakht, Anti-Atlas, Maroc, Bull. Mineral., 108, 551–574, 1985.

Fransolet, A.-M., Fontan, F., Keller, P., and Antenucci, D.: La serie johnsomervilleite-fillowite dans les associations de phosphates de pegmatites granitiques de L'Afrique-Centrale, Can. Mineral., 36, 355–366, 1998.

Fransolet, A.-M., Hatert, F., and Fontan, F.: Petrographic evidence for primary hagendorfite in an unusual assemblage of phosphate minerals, Kibingo granitic pegmatite, Rwanda, Can. Mineral., 42, 697–704, 2004.

Hatert, F.: Crystal chemistry of the divalent cation in alluaudite-type phosphates: A structural and infrared spectral study of the $Na_{1.5}(Mn_{1-x}M_x^{2+})_{1.5}Fe_{1.5}(PO_4)_3$ solid solutions (x = 0 to 1, $M^{2+} = Cd^{2+}, Zn^{2+}$), J. Solid State Chem., 181, 1258–1272, https://doi.org/10.1016/j.jssc.2008.02.035, 2008.

Hatert, F.: A new nomenclature scheme for the alluaudite supergroup, Eur. J. Mineral., 31, 807–822, doi.org/10.1127/ejm/2019/0031-2874, 2019.

Hatert, F., Roda-Robles, E., Keller, P., Fontan, F., and Fransolet, A.-M.: Petrographic significance of the triphylite + sarcopside intergrowths in granitic pegmatites: an experimental investigation of the $Li(Fe,Mn)PO_4$-$(Fe,Mn)_3(PO_4)_2$ system, Granitic pegmatites: the state of the art- International Symposium 6–12 May 2007, Porto, Portugal, 44–45, 2007.

Hatert, F., Baijot, M., and Dal Bo, F.: The stability of Fe-rich alluaudites in granitic pegmatites: An experimental investigation of the Na-Fe^{2+}-Fe^{3+} (+PO_4) system, Can. Mineral., 52, 351–371, https://doi.org/10.3749/canmin.52.2.351, 2014.

Hawthorne, F. C.: The crystal structure of morinite, Can. Mineral., 17, 93–102, 1979

Hawthorne, F. C.: Graphical enumeration of polyhedral clusters, Acta Cryst., A39, 724–736, 1983.

Hawthorne, F. C.: The minerals of the krohnkite supergroup: structural relations and chemical compositions, Mineral. Mag., 1–14, https://doi.org/10.1180/mgm.2025.2, online first, 2025.

Hawthorne, F. C. and Ferguson, R. B.: Refinement of the crystal structure of kröhnkite, Acta Cryst., B31, 1753–1755, 1975.

Hawthorne, F. C. and Pieczka, A.: Classification of the minerals of the graftonite group, Mineral. Mag., 82, 1301–306, doi.org/10.1180/minmag.2017.081.0923, 2018.

Heinrich, E. W.: Mineralogy of triplite, Am. Mineral., 36, 256–271, 1951.

Huvelin, P., Orliac, M., and Permingeat, F.: Ferri-alluaudite calcifere de Sidi Bou Othmane (Jelibet, Maroc), Notes due Service Geologique du Maroc, Rabat, 241, 35–49, 1972.

Kolitsch, U. and Fleck, M.: Third update on compounds with the kröhnkite-type chains: The crystal structure of wendwilsonite $[Ca_2Mg(AsO_4)_2 \cdot 2H_2O]$ and the new triclinic structure types of synthetic $AgSc(CrO_4) \cdot 2H_2O$ and $M_2Cu(Cr_2O_7) \cdot 2H_2O$ (M=Rb,Cs), Eur. J. Mineral., 18, 471–482, https://doi.org/10.1127/0935-1221/2006/0018-0471, 2006.

Krutik, V. M., Pushcharovskii, D. Yu., Pobedimskaya, E. A., and Belov, N. V.: Crystal structure of arrojadite, Sov. Phys. Crystallogr., 24, 425–49, 1979.

Losey, A., Rakovan, J., Francis, C. A., and Dyar, M. D.: Structural variation in the lithiophylite-triphylite series and other olivine-group structures, Can. Mineral., 42, 1105–1115, 2004.

Lottermoser, B. G. and Lu, J.: Petrogenesis of rare-element pegmatites in the Olary Block, South Australia, part 1. Mineralogy and chemical evolution, Mineral. Petrol., 59, 1–19, 1997.

Meusburger, J. M., Hudson-Edwards, K. A., Tang, C. C., Connolly, E. T., Crane, R. A., and Fortes, A. D.: Low-temperature crystallography and vibrational properties of rozenite ($FeSO_4 \cdot 4H_2O$), a candidate mineral component of the polyhydrated sulfate deposits on Mars, Am. Mineral., 108, 1080–1091, doi.org/10.2138/am-2022-8502, 2023.

Moore, P. B.: The crystal structure of metastrengite and its relationship to strengite and phosphosiderite, Am. Mineral., 51, 168–176, 1966.

Moore, P. B.: Crystal chemistry of the alluaudite structure type: Contribution to the paragenesis of pegmatite phosphate giant crystals, Am. Mineral., 56, 1955–1975, 1971.

Moore, P. B.: Sarcopside: Its atomic arrangement, Am. Mineral., 57, 24–35, 1972.

Moore, P. B.: Bracelets and pinwheels: A topological-geometrical approach to the calcium orthosilicate and alkali sulfate structures, Am. Mineral., 58, 32–42, 1973a.

Moore, P. B.: Pegmatite phosphates: Descriptive mineralogy and crystal chemistry, Mineral. Rec., 4, 103–130, 1973b.

Moore, P. B.: Pegmatite minerals of P(V) and B(III), MAC Short Course Handbook, 8, 267–291, 1982.

Moore, P. B. and Araki, T.: Atomic arrangement of merwinite, $Ca_3Mg[SiO_4]_2$, an unusual dense-packed structure of geophysical interest, Am. Mineral., 57, 1355–1374, 1972.

Moore, P. B. and Molin-Case, J.: Contribution to pegmatite phosphate giant crystal paragenesis: II. The crystal, chemistry of wyllieite, $Na_2Fe_2Al[PO_4]_3$, a primary phase, Am. Mineral., 59, 280–290, 1974.

Redhammer, G. J., Tippelt, G., Bernroider, M., Lottermoser, W., Amthauer, G., and Roth, G.: Hagendorfite $(Na,Ca)MnFe_2(PO_4)_3$ from type locality Hagendorf (Bavaria, Germany): crystal structure determination and ^{57}Fe Mossbauer spectroscopy, Eur. J. Mineral., 17, 915–932, https://doi.org/10.1127/0935-1221/2005/0017-0915, 2005.

Roda, E., Fontan, F., Pesquera, A., and Velasco, F.: The phosphate mineral association of the granitic pegmatites of the Fregeneda area (Salamanca, Spain), Mineral. Mag., 60, 767–778, 1996.

Roda-Robles, E., Pesquera, A., Garcia de Madinabeitia, S., Gil-Ibarguchi, J.-I., Nizamoff, J., Simmons, W., Falster, A., and Galliski, M. A.: On the geochemical character of primary Fe-Mn phosphates belonging to the trphylite-lithiophilite, graftonite-beusite, and triplite-zwieselite series: First results and implications for pegmatite petrogenesis, Can. Mineral., 52, 321–335, https://doi.org/10.3749/canmin.52.2.321, 2014.

Tait, K. T., Hawthorne, F. C., and Wise, M. A.: The crystal chemistry of the graftonite-beusite minerals, Can. Mineral., 51, 653–662, https://doi.org/10.3749/canmin.51.4.653, 2013.

Tait, K. T., Hawthorne, F. C., and Halden, N. M.: Alluaudite-group phosphate and arsenate minerals, Can. Mineral., 59, 243–263, https://doi.org/10.3749/canmin.2000057, 2021.

Tomes, H. E., Di Cecco, V. E., Tait, K. T., and Camara, F.: Crystal structure of near-endmember arrojadite-(BaNa) from Big Fish River, Yukon, Canada, Can. Mineral., 56, 923–938, https://doi.org/10.3749/canmin.1800018, 2018.

Vignola, P., Gatta, G. D., Hatert, F., Guastoni, A., and Bersani, D.: On the crystal-chemistry of a near-endmember triplite, $Mn_2^{2+}(PO_4)F$, from the Codera valley (Sondrio province, Central Alps, Italy), Can. Mineral., 52, 235–245, https://doi.org/10.3749/canmin.52.2.235, 2014.

Waldrop, L.: The crystal structure of triploidite and its relation to the structures of other minerals of the triplite-triploidite group, Z. Kristallogr., 131, 1–20, 1970.

Wise, M. A., Hawthorne, F. C., and Cerny, P.: Crystal structure of Ca-rich beusite from the Yellowknife pegmatite field, Northwest Territories, Can. Mineral., 28, 141–146, 1990.

Yakubovich, O. V., Siminov, M. A., Matvienko, E. N., and Belov, N. V.: The crystal structure of the synthetic finite Fe-term of the series triplite-zwieselite $Fe_2(PO_4)F$, Doklady Akademii Nauk SSSR, 238, 576–579, 1978.